Journal of Materials Research and Technology 33 (2024) 3714–3727

Contents lists available at ScienceDirect

Journal of Materials Research and Technology

journal homepage: www.elsevier.com/locate/jmrt

Characterization, generative design, and fabrication of a carbon fiber-reinforced industrial robot gripper via additive manufacturing

Selim Hartomacıoğlu [a,b,*], Ersin Kaya [a], Beril Eker [c], Salih Dağlı [d], Murat Sarıkaya [d,e]

[a] Department of Mechanical Engineering, Marmara University, 34722, Istanbul, Türkiye
[b] Department of Mechanical Engineering, Recep Tayyip Erdoğan University, Rize 53100, Türkiye
[c] Yildiz Technical University Science and Technology Application and Research Center, Davutpasa, Istanbul, Türkiye
[d] Department of Mechanical Engineering, Sinop University, Sinop, Türkiye
[e] Faculty of Mechanical Engineering, Opole University of Technology, 45-758, Opole, Poland

ARTICLE INFO

Keywords:
FDM
Mechanical testing
Generative design
Additive manufacturing
Industrial robot gripper
Optimization

ABSTRACT

Robot grippers are crucial components across various industrial applications, requiring special design and production for obtaining the optimal performance. Conventional plastic injection moulding techniques fall short in achieving the specificity needed for these grippers. To address this challenge, current paper focuses on developing a robot gripper using carbon fiber-reinforced polyamide with a next-generation composite filament and employing the innovative Generative Design technique. In the work, we began by characterizing and optimizing the composite material specifications. Then, the tensile strength and fracture mechanics of standard samples based on printing parameters, applying Taguchi experimental design for optimization were evaluated. Analysis of Variance (ANOVA) was used for factor analysis to fine-tune the process. Using the Generative Design technique, we determined optimal geometries, which were then fabricated through Fused Deposition Modeling (FDM). As a result, the optimization efforts led to significant improvements i.e., tensile strength increased from 103.2 to 116 MPa, and the elasticity modulus from 8386 to 8990 MPa. In practical industrial applications, we achieved a reduction in material weight from 14 to 4 g, lowered production costs from $5.16 to $1.50, and cut production time from 58 to 28 min. This study presents a validated method for developing industrial products with reduced material usage and costs, promoting sustainable production practices.

1. Introduction

The use of composite filaments in additive manufacturing (AM), also known as three-dimensional (3D) printing is rapidly increasing due to the increasing demand for advanced material properties such as high strength, long fatigue life and good energy absorption [1]. Both commercially available filaments and research into filament development play a critical role in the production and characterization processes. With low setup costs and a large selection of useable materials, fused deposition modeling (FDM) is the most popular extrusion-based AM technology. Using a heated nozzle of a specified diameter, thermoplastic filament is fed into the FDM process, and each layer is formed by the extruded material being deposited onto a bed that can also be heated for improved adherence [2–4].

The composite filament fabrication process is similar to the FDM process except that a fiber can be co-extruded with the plastic. Extensive research has recently been conducted on the integration of both continuous and staple fibers into composite filaments [5–7]. These studies generally include a range of fibers, such as glass fiber [8], carbon fiber [9] and Kevlar fiber [10], and focus on aspects such as fiber type and density. Moreover, research typically aims to optimize production parameters such as nozzle temperature, layer height, and 3D printing speed to evaluate their effects on tensile strength, impact strength, and microstructural properties [11–13].

Comprehensive literature research was conducted in this context. For instance, Tutar [14]studied the impact of production factors on the mechanical characteristics of polyamide (PA) and carbon fiber-reinforced PA materials that are manufactured by AM. The author highlighted that the addition of carbon fiber reinforcement boosted tensile strength and stiffness while decreasing toughness and ductility,

* Corresponding author. Department of Mechanical Engineering, Recep Tayyip Erdoğan University, Rize 53100, Türkiye
E-mail addresses: selimh@marmara.edu.tr (S. Hartomacıoğlu), ersin.kaya@marun.edu.tr (E. Kaya), beker@yildiz.edu.tr (B. Eker), sdagli@sinop.edu.tr (S. Dağlı), msarikaya@sinop.edu.tr (M. Sarıkaya).

https://doi.org/10.1016/j.jmrt.2024.10.064
Received 11 July 2024; Received in revised form 4 October 2024; Accepted 7 October 2024
Available online 9 October 2024
2238-7854/© 2024 The Author(s). Published by Elsevier B.V. This is an open access article under the CC BY-NC-ND license (http://creativecommons.org/licenses/by-nc-nd/4.0/).

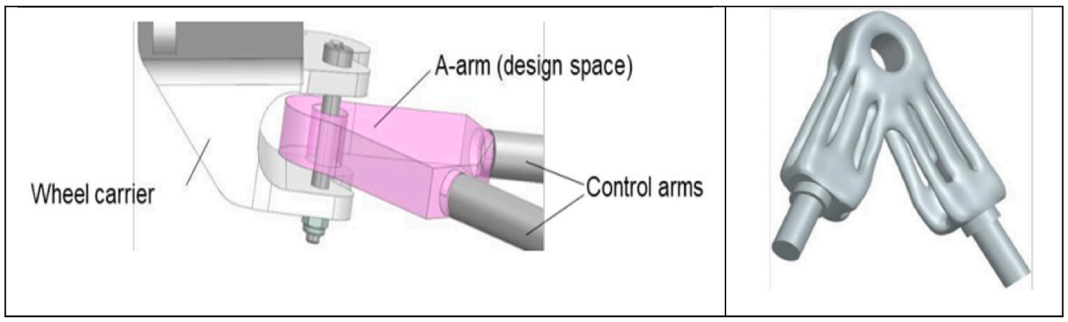

Fig. 1. A-arm design conducted by Generative Design Approach [27].

irrespective of the raster angle. Condruz et al. [15] examined the mechanical characteristics of three thermoplastic-based materials that are readily accessible for use in the fused filament deposition (FFD) process. It was found that UltraFuse polyamide high temperature carbon fiber reinforced with 15% has the best mechanical performances. Tavara et al. [16] examined the effects of anisotropy and ageing on the mechanical properties of 3D printed short carbon fiber–reinforced polyamide composites. The study used 100% infill samples that were produced and subjected to tensile and fracture toughness tests. The filament material contained 12.8% short carbon fiber particles and knitted in +45/-45 configurations. Venkatesh et al. [17] investigated the effect of adding carbon fiber to polylactic acid (PLA), acrylonitrile butadiene styrene (ABS), and nylon on mechanical features. They considered the nozzle temperature, infill line directions, and carbon fiber addition as variables and determined the Young modulus and tensile strength as research outputs [2]. Chacón et al. [18] studied the effect of production parameters such as build orientation, layer thickness, and fiber volume content on continuous fiber-reinforced thermoplastic composites in terms of mechanical properties. FDM 3D-printed parts consisting of carbon, kevlar, and glass fibers were fabricated at two different build orientations i.e., flat and on-edge build orientations. Tensile and 3-point bending tests were carried out to investigate mechanical properties, and fractured surfaces were evaluated using scanning electron microscopy (SEM) images. Their findings indicated that flat specimens had greater values of strength and stiffness than on-edge specimens and that carbon fiber reinforced composites had the highest mechanical performance with higher stiffness. Caminero et al. [19] observed the impact damage performance of continuous fiber-reinforced thermoplastics and analyzed the impact strength obtained from Charpy tests. Also, researchers studied the effects of build orientation, layer thickness, and fiber volume fraction on the results. According to findings, in flat samples, impact strength rose with increasing layer thickness; in on-edge samples, however, impact strength fell, indicating a more brittle fracture. Ferreira et al. [20] performed low-speed impact tests to study the ageing effect of continuous carbon fiber-reinforced composites produced by fused deposition modelling. Findings indicated that the original elastic component shrinks slightly with age. Furthermore, it was evident from the specimens that the degree of vision impairment changed with age. Ferreira et al. [21] conducted a review study for producing fiber-reinforced composites via the FDM method. They compiled the papers on composites with different matrix materials and continuous or discontinuous reinforcement fibers. Also, researchers classified them according to different fiber types, matrices, fiber densities and production types. They stated that some of these limitations were addressed by the development of different options i.e., the formulation of high-performing polymers, the FFF technique for creating fiber-reinforced materials, and/or the design of new FFF-based processes for composite material manufacturing. Prajapati et al. [22] observed the effects of build orientation, fiber angle, and number of fiber rings on impact resistance. They used glass fiber-reinforced filament, and samples with 0°/90° and ±45° fiber angles were produced and then, tested. They used glass fiber-reinforced filament, and samples with 0°/90° and ±45° fiber angles were produced and tested. AlMuhanna and AlMangour [23] conducted a study to examine the effect of building orientation and fiber type on the mechanical behaviour of additively manufactured ABS matrix composites. Glass fiber and carbon fiber reinforced ABS samples were produced in flat, on-edge, and up-right building orientations. The results showed that building orientation greatly effects a number of mechanical features. Also, the most desirable mechanical characteristics were created by buildings oriented in-plane, or flat and on the edge, whereas the poorest mechanical values were produced by buildings oriented upright. Kabir et al. [24] aimed to maximize the performance of fiber-reinforced nylon composites produced by the FDM method. Several important factors, such as fiber orientation, the volume of fiber filament, the volume of polymer filament, the fiber volume fraction of composite, estimated weight and measured weight values were studied. Findings showed that, despite the fact that 3D printed composites are naturally defective in that they feature voids, which can cause the composites to fail prematurely, fiber orientation with the highest possible fiber content significantly improves the performance of the composites. Another review study was conducted by Wickramasinghe et al. [25]. The focus of the study is on fiber-reinforced composites (FRC), which are essentially examined in two separate groups: continuous and discontinuous fiber reinforcements. In this comprehensive literature review, papers were evaluated in terms of parameters such as layer thickness, infill pattern, raster angle, and fiber orientation. As a result, there are two possible values for the ideal raster angle to attain the maximum tensile strength in polymers: 0° and 90°. Nagendra and Prasad [26] studied optimizing some important production parameters such as layer thickness, 3D printing temperature, raster angle, infill part density, and infill pattern of nylon-aramid fibers composite used as a filament material. Parameters such as layer thickness, 3D printing temperature, raster angle, infill part density, and infill pattern style were investigated and optimized using the Taguchi technique.

Generative Design has become widespread in the industry due to the rapid development of AM technology. Artificial intelligence-based software creates alternative designs for products and create geometric structures in accordance with load and boundary conditions. For instance, in the investigation undertaken by Junk and Rothe [27], a Generative Design component was manufactured. This component, leveraging fiber-based filament, facilitated the creation of an A-arm of the rear axle of the racing car, thereby offering notable advantages in terms of weight reduction and production cost optimization. The product and the newly generated model from the study are illustrated in Fig. 1.

The design and integration of cross-joint components into AM processes were investigated on Generative Design conducted by Han et al. [28]. The study highlighted that the integrated approach would reduce production cycle times and enhance production quality. Initially, numerous models were automatically generated based on the first geometry prepared using machine learning-based Generative Design

Table 1
The selected experimental parameters and their levels (input parameters).

Symbol	Parameters	Unit	Level 1	Level 2	Level 3
A	Nozzle temperature	°C	240	260	280
B	3D printing speed	mm/s	30	55	80
C	Heat treatment time	min	0	20	40

algorithms. Subsequently, the models were evaluated based on design criteria and cost, verified through finite element analysis, and manufactured using the FDM technique.

In summary, while much of the existing literature emphasizes material development and the optimization of production parameters, there is a notable gap in the application of statistical experimental design and subsequent optimization for samples produced with carbon fiber-reinforced filaments, particularly concerning their commercial viability.

The present paper intends to address this gap by optimizing both material properties and production parameters. Following optimization process, Generative Design which is an advanced design methodology applied to a commercial product. The research employs an experimental development approach, with analytical models used to interpret the results. This dual focus on optimization and productivity enables increasing the usability of carbon fiber-reinforced filaments in practical and commercial applications.

2. Materials and methods

The study was conducted in three distinct stages, beginning with the characterization of the CF15 (15 wt% carbon fiber) reinforced PA material. During the initial stage, samples produced under various manufacturing parameters were subjected to tensile testing to assess their mechanical performance. The research follows an applied methodology, utilizing 15 wt% carbon fiber particle-reinforced Nylon6 for the development of the robotic gripper. Filament materials were obtained from BASF-Germany. The extrusion diameter of the filament was 2.85 mm, and the diameter of the nozzle used for extrusion was 0.6 mm. Mechanical properties of materials supplied by the manufacturer can be found in Table S1.

In this study, an Ultimaker S5 FDM 3D printer with a build volume of 330 x 240 × 300 mm, capable of working with high-strength glass and carbon filaments, and a layer resolution of 20 μm was used. The samples were printed on a glass plate using a special adhesive to ensure adhesion. Tensile test specimens were produced in accordance with ASTM D683-14 Type I standard. All sample data was formatted in.stl format facilitating integration into the printing process. A production plan was developed based on the initial dimensions of the samples shown in Fig. S1. The production process was organized using Ultimaker Cura 5.3.0 software. After the design was sliced, the G codes were transferred to the 3D printer to begin production.

Table 3
Performance-cost analysis.

No	Force [N] (1 mm Deformation] FDM	Weight [g]	Production time [min]	Cost [$]
1	182.50	4	28	1.50
2	212.50	5	28	1.86
3	185.00	8	39	3.00
4	192.50	9	40	3.39
5	***Cancel***	4	25	1.50
6	225.00	12	54	4.50
7	***Cancel***	4	26	1.50
8	72.50	4	24	1.50
9	177.50	14	58	5.16

Taguchi method was used during the experimental design phase. This method begins with a comprehensive factor analysis in which production parameters are systematically ranked and prioritized. For this study, specific parameters including nozzle diameter, table temperature and filler type were set as fixed values, i.e. 0.6 mm, 100 °C and 'concentric' respectively. Key parameters for inclusion in the experimental design were identified based on constraints including insights from preliminary experiments and production cost considerations.

The respective level values corresponding to the selected parameters were gleaned from both manufacturer catalogue data and preliminary experiments. Additionally, in this work, in order to strengthen the bond between layers, heat treatment was carried out by keeping the products in a temperature environment of 80 °C for a certain period of time. The identified parameters and their corresponding specifications are presented in Table 1.

Considering the parameters and number of levels given in Tables 2 and 3ˆ3 = 27 experiments are required for a full factorial experiment in the statistical experimental design method. However, due to the difficulty of performing the tests and the high production cost, it is aimed to find the optimum parameters with a smaller number of experiments. For this purpose, the Taguchi optimization method has been used. In the Taguchi experimental design method, for a study with 3 factors and 3 levels, an L_9 experiment is recommended. With the selected L_9 experimental design table, 8 effects and interactions can be calculated. Three

Table 2
ANOVA results for weight, tensile strength, and surface roughness.

Weight	Source	DF	Adj SS	Adj MS	F-Value	P-Value	% Contribution
	A	2	0.1344	0.0672	93.06	0.011	50.25
	B	2	0.1083	0.0541	75.05	0.013	40.52
	C	2	0.0232	0.0116	16.10	0.058	8.69
	Error	2	0.0014	0.00072			0.54
	Total	8	0.2674				100
R^2: 99.46%							
Tensile strength	Source	DF	Adj SS	Adj MS	F-value	P-value	% Contribution
	A	2	209.41	104.73	11.59	0.079	49.94
	B	2	173.38	86.69	9.60	0.094	41.35
	C	2	18.48	9.24	1.02	0.494	4.40
	Error	2	18.06	9.03			4.31
	Total	8	419.34				100
R^2: 95.69%							
Surface roughness	Source	DF	Adj SS	Adj MS	F-value	P-value	% Contribution
	A	2	3697.7	1848.84	34.23	0.028	53.10
	B	2	2870.7	1435.36	26.57	0.036	41.23
	C	2	286.1	143.06	2.65	0.274	4.12
	Error	2	108.0	54.01			1.55
	Total	8	6962.5				100
R^2: 98.45%							

(DF: Degree of freedom, Adj SS: Adjusted sums of squares, Adj MS: Adjusted mean squares).

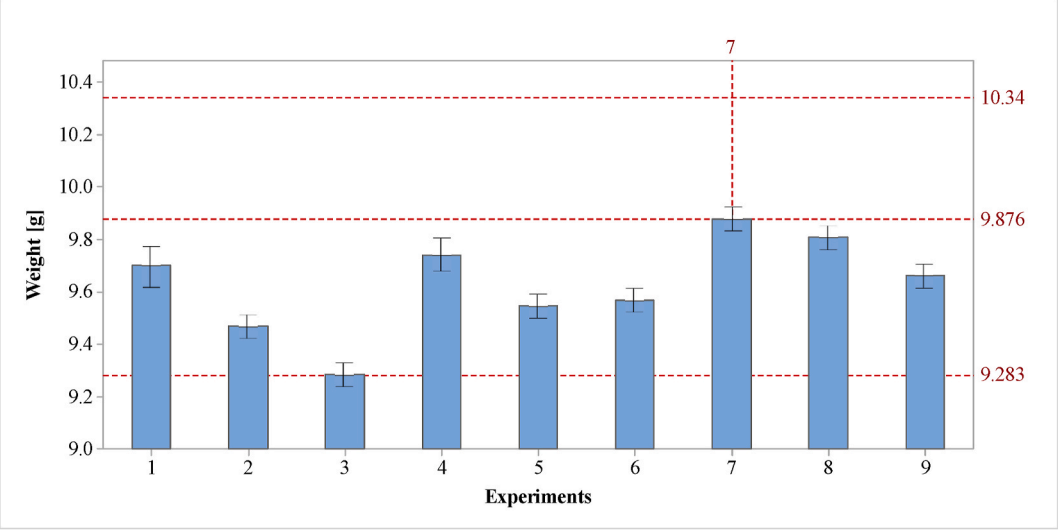

Fig. 2. Samples' weights obtained from experimental study.

of these are main effects, called A, B and C, and the remaining 4 are interactions and their equivalents. The tensile strength value obtained in the study was accepted as the main response variable. The selected experimental design (L_9 orthogonal array) is given in Table S2.

In this study, after obtaining the experimental data, the signal-to-noise (S/N) ratios were calculated to analyze the optimum points and the effect of parameters on the responses. Since the study's primary objective is to increase the strength value and to reach the theoretical density of the reference material, the 'higher-the-better' approach has been employed. According to this method, the S/N ratio for each experiment was calculated using Eq. (1). Here, a higher signal-to-noise ratio is desired, indicating a lower noise ratio. The noise ratio encompasses uncontrollable factors like machine vibration, flow rate, non-homogeneous material regions, and irregular speed. The data obtained from the applied method has been graphed and evaluated.

$$\frac{S}{N} = -10\,log\left(\frac{1}{n}\sum_{i=1}^{n}\frac{1}{y^2}\right) \tag{1}$$

Where i = 1,2,3 ….n, Y is output values of response.

In the study, to facilitate a detailed evaluation and interpretation of the results, the unperformed experiment outcomes were estimated. Following the prediction process in the Taguchi experimental design method, the data were evaluated and graphed. The prediction model used in the study is provided below (Eq. (2)):

$$\eta_{opt} = \eta_m + \sum(\overline{\eta}_i - \eta_m) \tag{2}$$

Where η_m = the overall mean of signal-to-noise ratio, f = the number of factors, η_i = the mean of signal-to-noise ratios at the optimal level of each factor i.

In this study, ANOVA method was utilized to investigate and evaluate the effects of factors on the result. General Linear Model was used for analysis and then F and P values were calculated for each factor and error. Furthermore, the effects of the factors were determined in terms of percentage error. A P-value greater than 0.05 indicates a significant effect of the experimental parameter. F, P, and percentage error values were computed and tabulated for each factor. Each sample produced within the scope of the study was numbered and packaged separately. Subsequently, the weight of each sample was measured with a precision balance and detail.

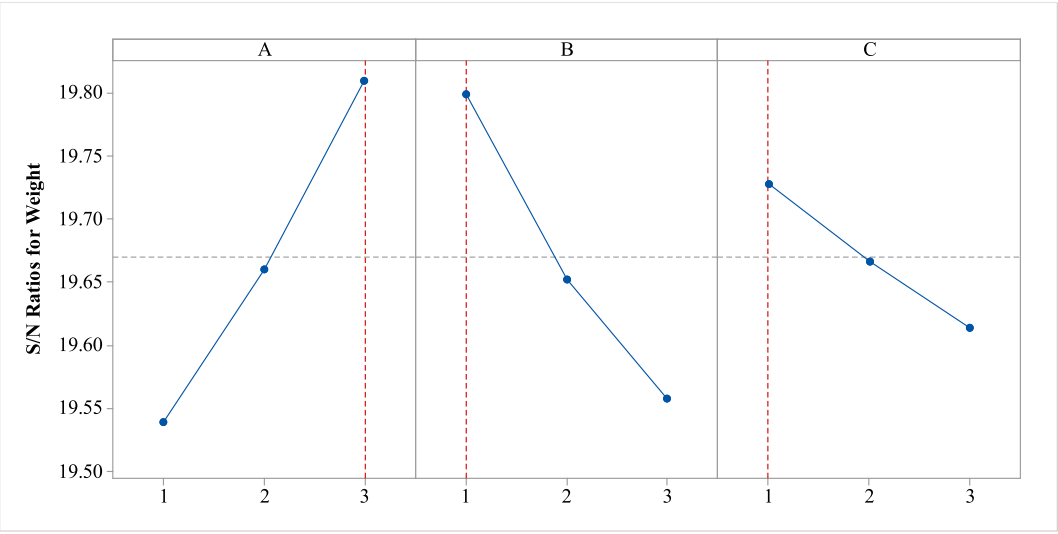

Fig. 3. S/N ratios for samples' weight values.

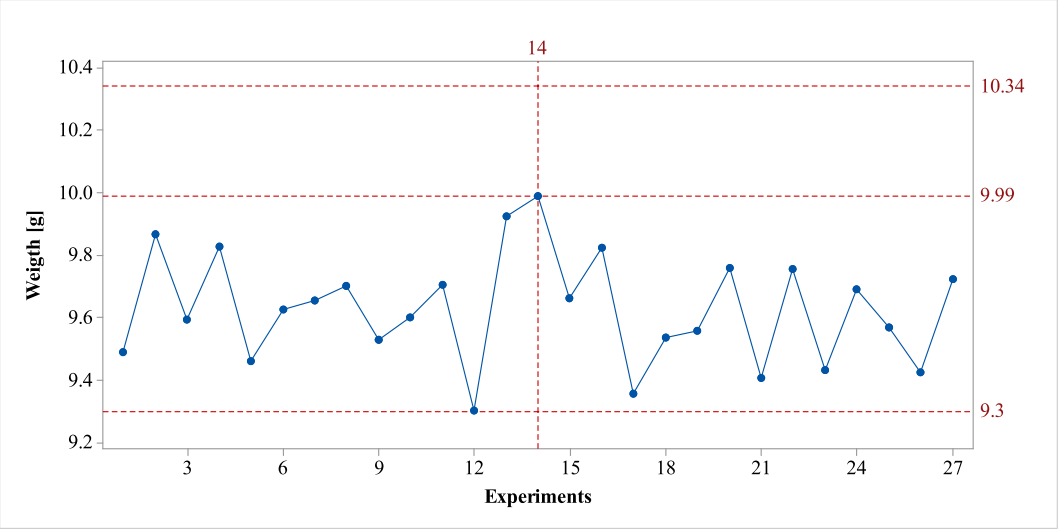

Fig. 4. Estimated weight values of samples.

3. Results and discussion

3.1. Characterization and optimization of production parameters

Weight is an important parameter in AM processes in terms of performance. After conducting a study, it was observed that, despite having the same printed geometry, the weights of the samples varied. Fig. 2 presents the average weight results. When Fig. 2 is examined, it can be concluded that the highest weight of 9.88 g was obtained in experiment 7, where the nozzle temperature was set to 280 °C, the 3D printing speed was 30 mm/s, and the heat treatment time was 40 min. The results indicated that higher nozzle temperatures caused the molten material to spread more, resulting in a decreased porosity rate and an increased sample weight. The sample weight was expected to be 10.34 g, based on the theoretical density and the sample volume of 8.39 cm^3. However, the actual sample weights varied, and the largest error amount was observed in experiment 3. The lowest error rate was recorded in experiment 7, at 4.49%. Similar results have been obtained in the literature and the reason for this situation has been evaluated from various perspectives. For example, in a study conducted on maximizing the performance of fiber-reinforced composites produced by 3D printing, it was observed that there was a difference between the calculated and measured weights, and here factors such as fiber orientation and other parameters were effective [24]. In another study, conclusions drawn from the results indicated notable differences in weight among the samples, with infill density emerging as the most critical parameter for weight variation [29].

Fig. 3 shows the signal-to-noise (S/N) ratio for each experimental parameter. Each graph shows notable variations, highlighting the significant impact of selected parameters and their levels on weight. The best parameters identified are A_3, B_1 and C_1. The P value and percentage effect indicating the significance level of each factor were determined using ANOVA analysis as listed in Table 2. The parameters, i.e., A (nozzle temperature) and B (3D printing speed), exhibited P values less than 0.05, indicating a significant level of significance. In contrast, parameter C (heat treatment time) had a P value of 0.058, corresponding to a significance level of 8.69%. The effect of nozzle temperature was calculated as 50.25%, 3D printing speed as 40.52% and heat treatment time as 8.69%. Experimental error was measured as 0.54%. The regression model showed robust prediction accuracy for the experimental data with an R-squared value of 99.46%.

The optimal parameter, which was not in the L_9 experimental design table, was estimated using the full factorial experimental design table. According to the estimation, the experiment closest to the expected weight is experiment $A_3B_1C_1$ (14th experiment), with a calculated value of 9.99 g. It has been determined that the deviation of this value from the expected weight is 3.38%. The weights obtained from the estimation are provided in Fig. 4. In the study's characterization step, the products' mechanical properties were examined. Stress-strain graphs obtained from the tensile testing process are provided in Fig. 5. Young's modulus, tensile strength, and elongation have been calculated and are presented in Figs. 6 and 7, respectively.

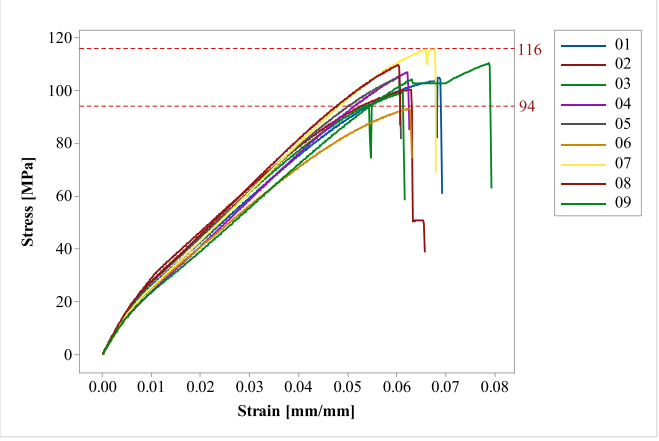

Fig. 5. Stress-strain curves for samples.

According to the results of weight training, Young modulus and tensile strength values reached their maximum in the 7th experiment. This shows that there is a significant correlation between weight and mechanical properties, which are vital for printing performance. In terms of percentage elongation at break, it was seen that the highest value occurred in the 1st experiment and the lowest value occurred in the 9th experiment. The optimization of present work was made based on tensile strength values with parallel evaluations. Initially, Taguchi analysis was conducted using a 'higher is better' approach. After analysis, S/N ratios were calculated for each experiment and effect graphs were drawn. A graphical representation of the results can be found in Fig. 8 and 9. As seen from the graph, the optimal production parameters for tensile strength value are determined to be $A_3B_1C_2$. The graph also indicates that the nozzle temperature (parameter A) has the most significant impact on the outcome, followed by printing speed (parameter B), while heat treatment time (parameter C) has the least effect. ANOVA

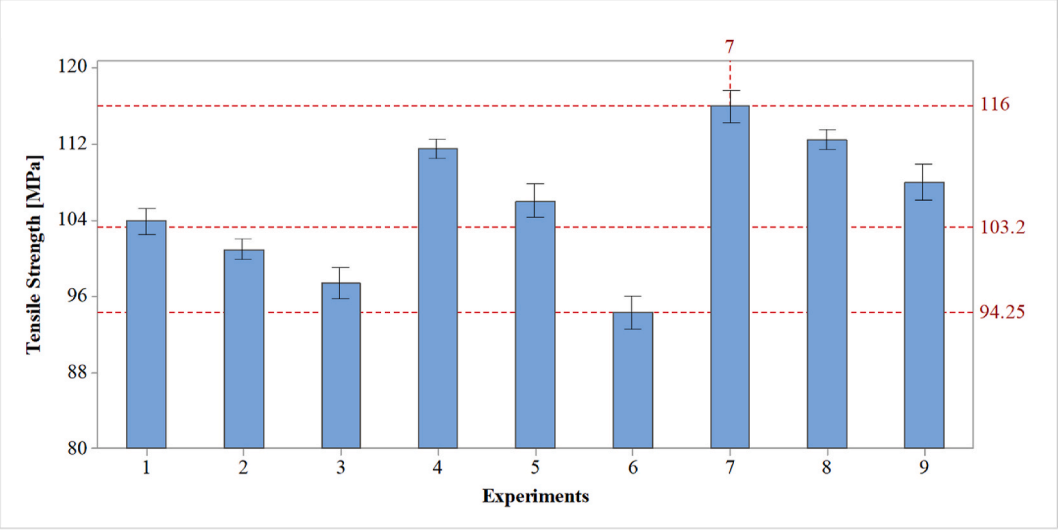

Fig. 6. The change of tensile stress values as per experiment number.

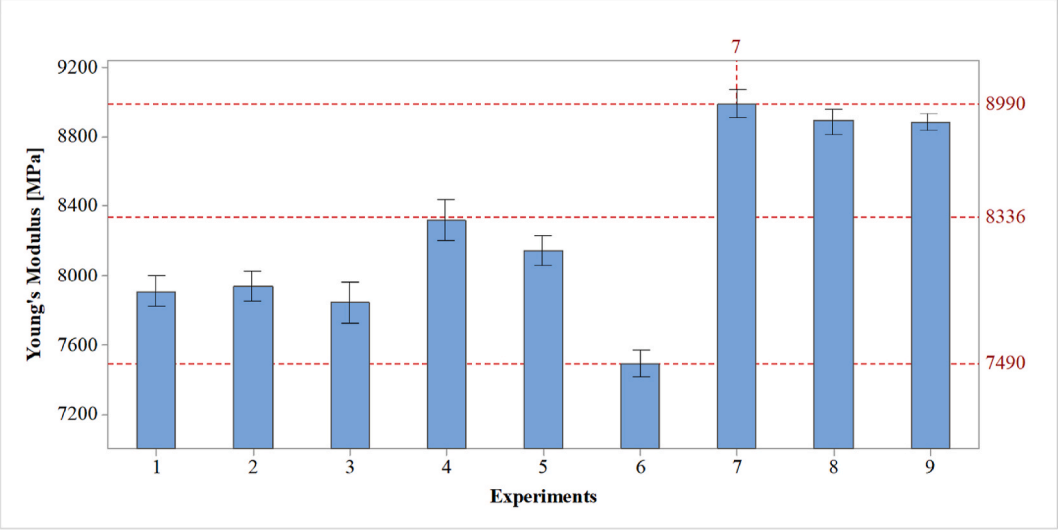

Fig. 7. The change of Young's modulus as per experiment number.

analysis was also conducted for the Tensile Strength. According to the results of the ANOVA study, the error value in the experiment is 4.31%. The most significant effect is attributed to parameter A (49.94%), followed by parameter B (41.35%) and parameter C (4.40%). The P-values indicate that the significance levels for parameters A, B and C are 0.079, 0.094 and 0.494, respectively. The generated model has an R^2 value of 95.69%, indicating that the model is highly accurate in predicting outcomes.

In this study, the model was developed using a full factorial experimental design based on 27 experiments. Fig. 10 displays the predicted tensile strength values. The highest tensile strength is observed for the parameter combination $A_3B_1C_2$, followed by $A_3B_1C_3$. While the combination A_3B_1 remains consistent, the third parameter, C (heat treatment time), shows minimal impact on the tensile strength. The specific levels of heat treatment time tested did not yield a significant effect. Consequently, further investigations are required to assess the influence of varying heat treatment temperatures and durations.

Fig. 11 depicts the damage states of the samples following tensile testing, revealing that all samples exhibited brittle fracture characteristics. SEM images from experiment No. 1, shown at varying magnifications in Fig. 12, illustrate both fractured and intact surfaces. Analysis indicated that the observed damage is mainly due to the detachment and rupture of carbon fibers from the Nylon6 matrix and the subsequent separation of the matrix material. Usually, Nylon6 presents a tensile strength and an elongation at break of approximately 55 MPa and 100%, respectively [17]. The incorporation of 15% discontinuous carbon fibers increases the tensile strength to 116 MPa but reduces the elongation to 1.78%, highlighting a substantial improvement in tensile stiffness and strength.

Comparative studies from the literature report that continuous carbon fiber reinforcement achieves a tensile strength of 700 MPa with 1.2% elongation [21], whereas specimens reinforced with 12.8% chopped carbon fibers yielded a tensile strength of approximately 55 MPa [16]. Manufacturer data for longitudinally woven filaments indicate a tensile strength of 103.2 MPa with 1.8% elongation. A detailed examination of these studies suggests that continuous carbon fiber reinforcement substantially enhances tensile strength, although the improvement is less pronounced in products reinforced with chopped fibers. From a production standpoint, filaments reinforced with chopped fibers offer greater convenience for filament production and product fabrication. The current study demonstrates that by optimizing production parameters, the resulting product can significantly surpass the

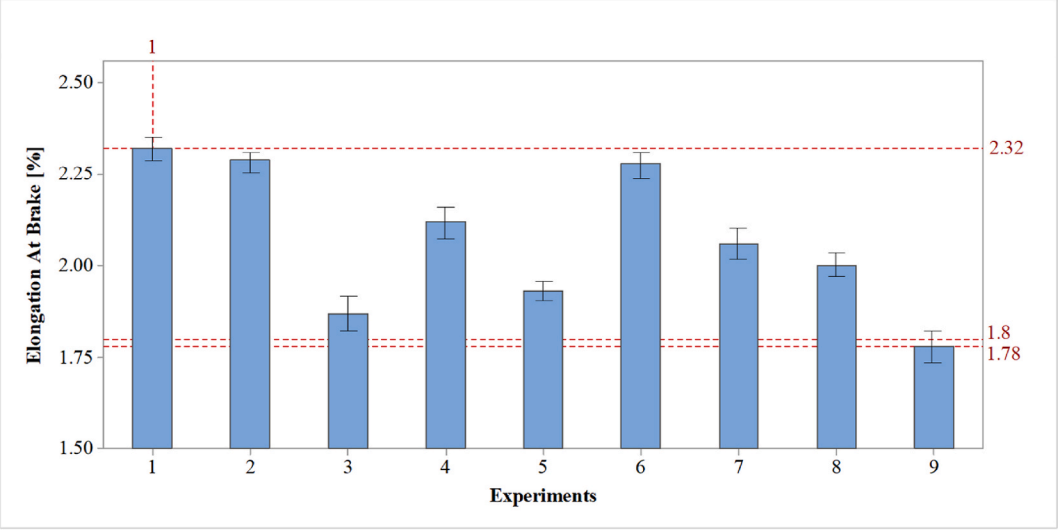

Fig. 8. The change of elongation at brake (%) as per experiment number.

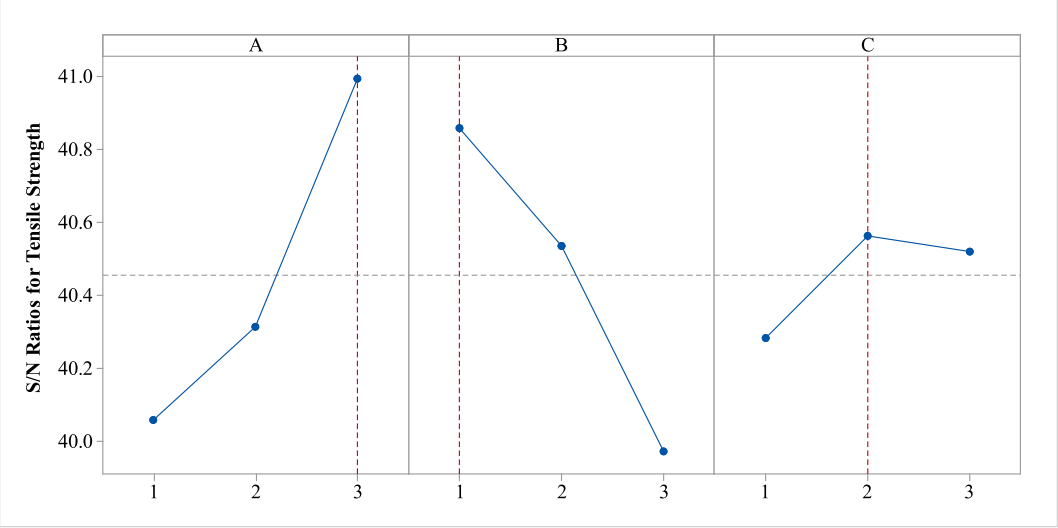

Fig. 9. S/N ratios for samples' tensile strength.

specified mechanical properties.

In conclusion, when evaluated in terms of both weight and tensile strength, parameter $A_3B_1C_2$ was selected for production. Fracture mechanics were analyzed at the final characterization stage. Accordingly, after the tensile tests performed to examine the mechanical properties of the samples, SEM images were taken at different magnifications perpendicular to the fracture surfaces of the composite samples in order to perform damage analysis. The effects of carbon fiber reinforcement in terms of mechanical properties and damage development on Nylon6 matrix samples were examined and damage modes were determined. As a result of the damage analysis, it was seen that the different toughening mechanisms created by the carbon fiber reinforcement in the samples affected the damage development. In addition, damage modes such as ductile fracture surfaces, brittle fracture surfaces, macro and micro matrix cracks, matrix fibrillation, debonding and pull-out were identified and interpreted.

SEM images of the samples are given in Fig. 12. When SEM images are examined, it is seen that multiple macro and micro cracks are formed. Additionally, these cracks extended into the sample and a rough fracture surface was formed. This situation positively affected the damage development mechanisms and caused the strength and toughness of the material to increase. However, gradual crack damage occurred and debonding and pull-out damage was observed in the fibers in this crack area. In addition, matrix fibrillation on broken surfaces due to the effect of intense shear stress and plastic deformation on damaged surfaces is noteworthy. When the SEM images were examined in detail, it was determined that a good interface was formed between the fiber and matrix components as a result of the thermoplastic fibers containing chopped fibers melting and solidifying again under the influence of temperature. While no secondary breakage damage occurred in the clipped fibers on the damage surfaces, intense fiber pull-out damage was observed on the breakage surfaces.

In this study, Keyence digital optical microscope was employed in order to examine the surfaces of the samples. Measurements were systematically taken and recorded from consistent regions in all samples. Initial analyzes focused on transition points between layers, and 3D surface topography images were captured to visualize these areas. An example of 3D surface topography and optical microscope surface images is shown in Fig. 13. The surface roughness values obtained from nine experiments are shown in Fig. 14.

Based on the results presented in Fig. 14, the highest surface roughness value was observed in the 9th experiment. This means the

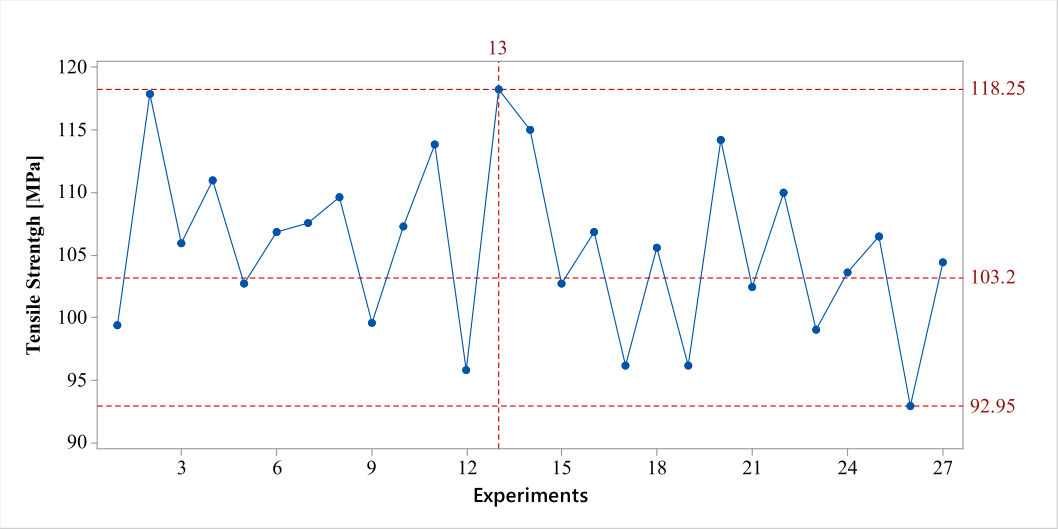

Fig. 10. Estimated tensile strength values.

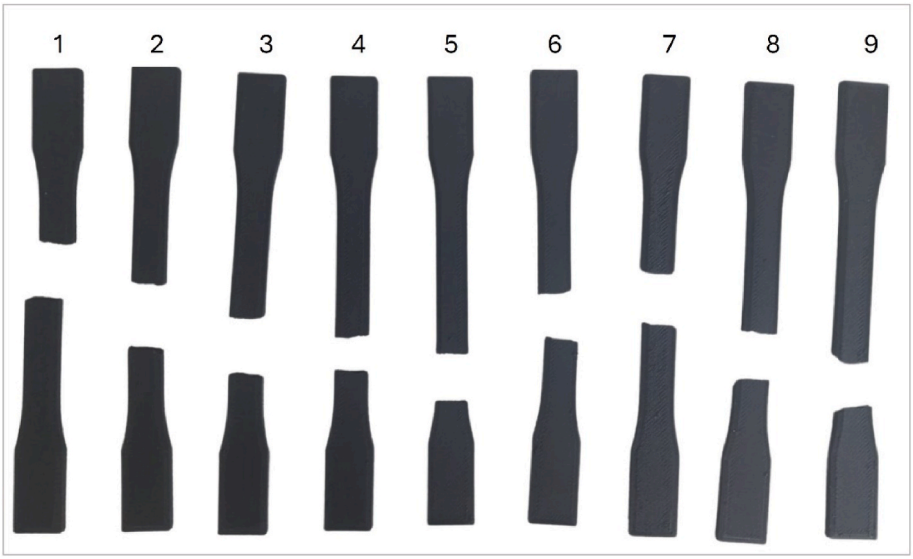

Fig. 11. Fracture behavior of samples subjected to tensile testing.

parameter set with a nozzle temperature of 280 °C, 3D printing speed of 80 mm/s, and thermal treatment duration of 20 min. On the other hand, the lowest surface roughness was obtained in the 2nd experiment, where a nozzle temperature of 240 °C, 3D printing speed of 55 mm/s, and thermal treatment duration of 20 min were used. Contrary to the values of weight and tensile strength, as seen from the table and values, medium values of 3D printing speed and high printing temperature resulted in better surface roughness.

The S/N ratios were computed to obtain the optimum parameter combination and evaluate their impact on surface roughness. These ratios were subsequently handled to create effect graphs, as drawn in Fig. 15. As consistent with previous observations, nozzle temperature exhibited the most substantial impact on surface roughness, followed by 3D printing speed and heat treatment time which has a negligible effect. Unlike the effect graphs for weight and tensile strength, where parameter B provided the maximum S/N ratio at the first level, it provided the maximum S/N ratio for surface roughness at the second level. This suggests that a 3D printing speed of 55 mm/s results in superior surface roughness.

Based on the S/N ratios obtained in this study, the optimal parameters for minimizing surface roughness were determined to be $A_1B_2C_3$. The ANOVA analysis results presented in Table 2, which follow the surface roughness data derived from the effect graph, show that the P-values for parameters A and B are less than 0.05, indicating statistically significant effects. Conversely, parameter C has a P-value of 0.274, consistent with the effect graphs, indicating a low level of significance. When the impacts are expressed as percentages, parameter A accounts for the highest influence at 53.1%, parameter B follows with 41.23%, and parameter C has the least impact at 4.12%. Experimental error has a negligible percentage effect of 1.55%.

Initially, the experimental work required 27 full factorial experiments. However, to simplify the process, the experimental load was reduced to one-third of the original by using the L_9 orthogonal array. After analysis and optimization, mathematical modeling predicted the results of 27 experiments, as shown in Fig. 16. Accordingly, Fig. 16 shows that the optimum parameter combination ($A_1B_2C_3$) achieves the minimum surface roughness value of 53.09 μm.

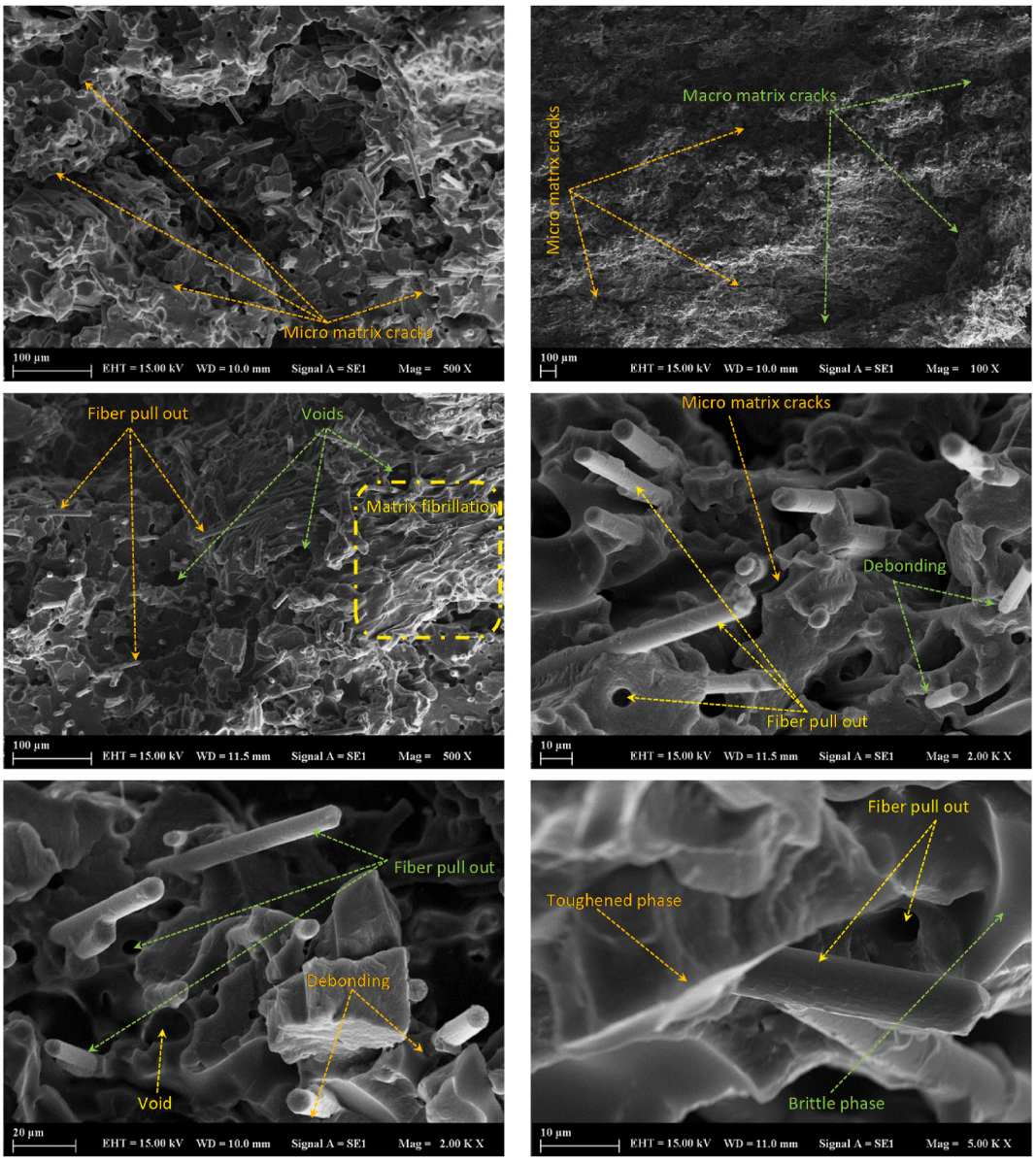

Fig. 12. The SEM images of fractured surfaces at different magnifications.

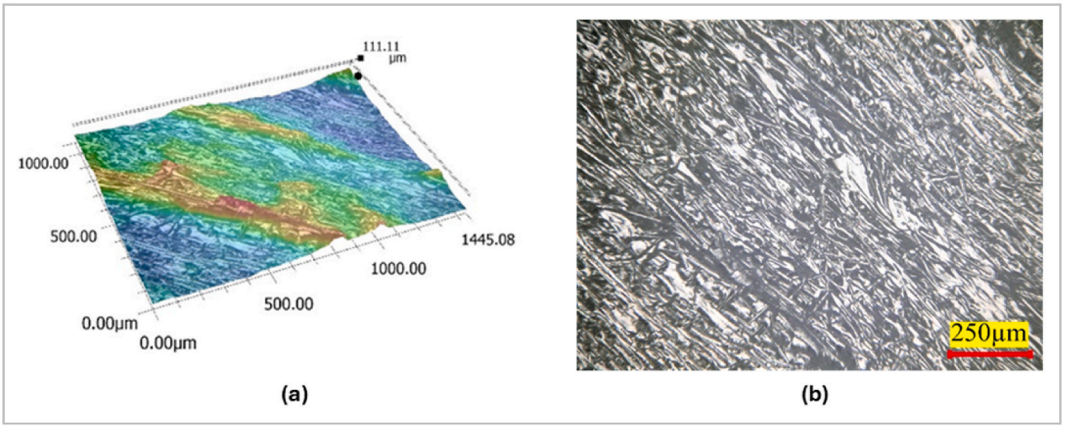

Fig. 13. a) 3D surface topography and b) optical image of the sample obtained in experiment No. 1.

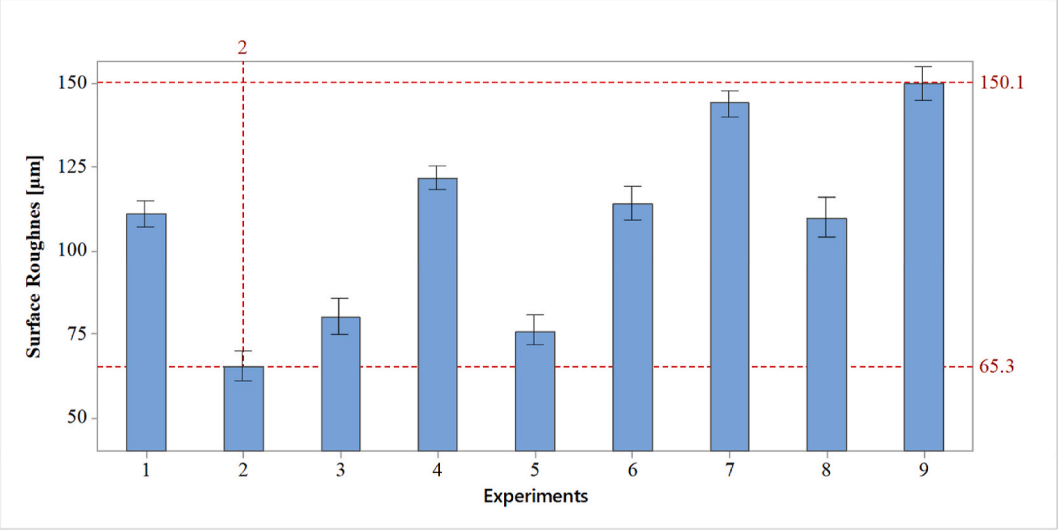

Fig. 14. Surface roughness results of the samples.

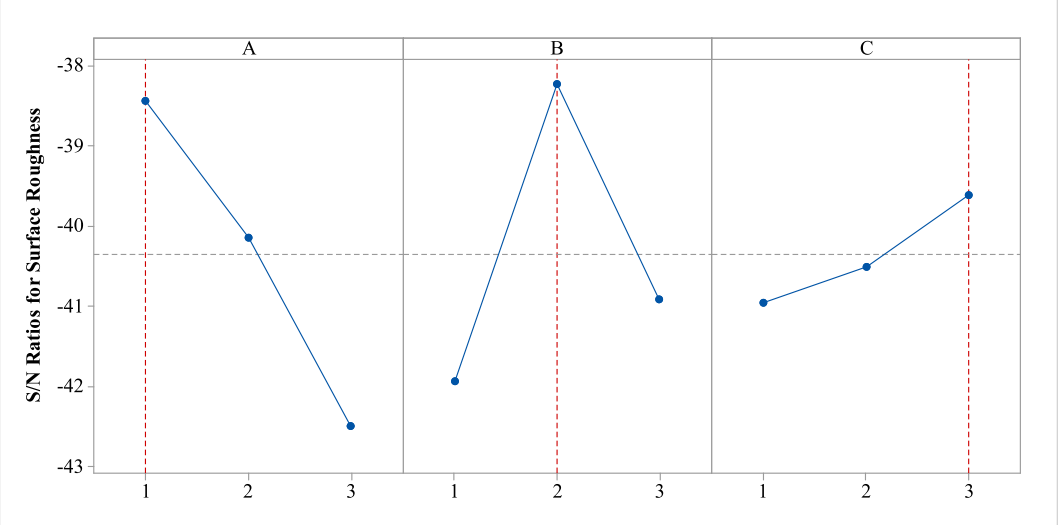

Fig. 15. S/N ratios for surface roughness values.

3.2. Generative Design and fabrication of industrial robot gripper

The present study comprises two distinct parts. The first part focuses on investigating and optimizing the production parameters of a material. In the second part, a robot gripper intended for industrial applications was developed. These grippers are specifically designed for particular workpieces in automation systems and are typically produced in small batches due to their specialized nature. Generally, these grippers have been designed via conventional 3D design methodologies and manufactured using metal forming and/or machining processes [30]. However, thanks to the advancement of design manufacturing technologies as well as manufacturing processes, there is a growing need to adopt alternative approaches that are more cost-effective, utilize less material, and offer enhanced design capabilities [31,32]. To address this need, this study developed gripper designs for industrial robots based on the principles of Generative Design. Following the design phase, the grippers were manufactured using carbon fiber-reinforced nylon which is a next-generation material, and then, they were tested in a specially designed test setup.

In this work, Autodesk Fusion 360 software was used in the Generative Design stage. First, the existing gripper 3D model was designed and dimensioned as can be seen in Fig. 17. As illustrated in the figure, the carrying capacity of a product with the given dimensions is 150 N.

In the Generative Design process, the initial step involves identifying the fixed regions where the structure will interface with external elements. In present work, areas highlighted in red were designated as fixed, indicating the regions where the gripper will secure the part. Similarly, the areas marked in green were also treated as fixed points, as they will be used for screw connections. All other areas were considered adaptable and subject to optimization. Then, FDM was selected as the production method. The primary objective of the study is to minimize the mass of the gripper while ensuring a safety factor of 2. The optimized material parameters obtained from the preceding section were utilized as the basis for determining the safety factor. Stress analysis was conducted using the Von Mises stress criterion (refer to Fig. 18), as defined by the corresponding formula.

Autodesk Fusion 360 software, equipped with an artificial intelligence-based Generative Design module, has generated various geometries based on constraints and materials. Eight different geometry alternatives have been produced, as shown in Fig. 19.

The obtained geometries and the initial model were planned for production using Ultimaker Cura software with 15% carbon fiber

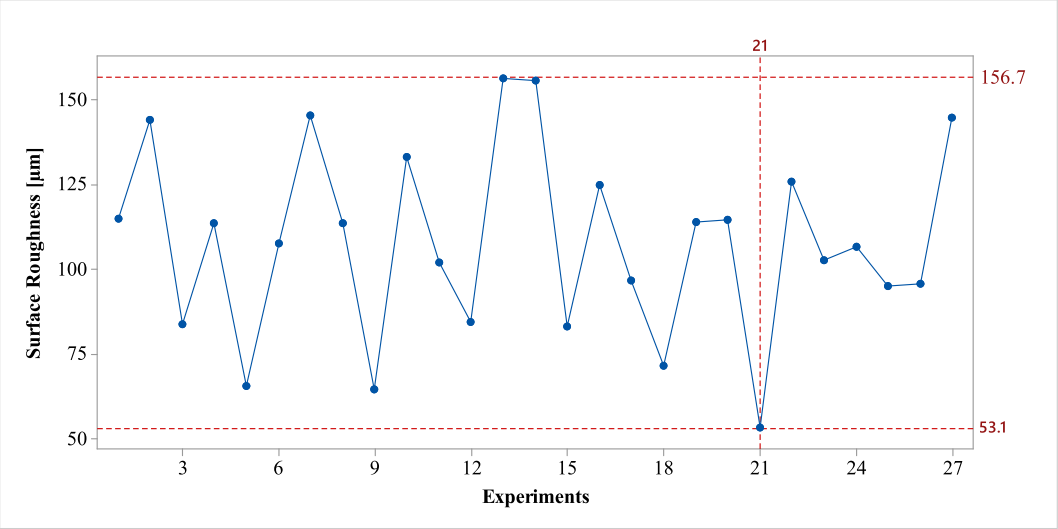

Fig. 16. Estimated surface roughness values of samples.

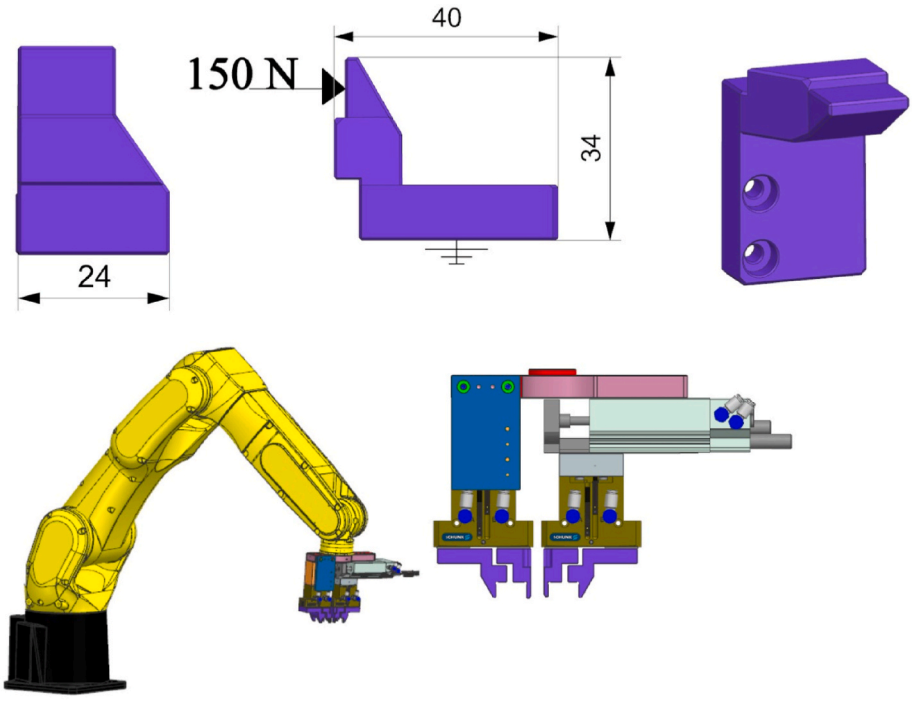

Fig. 17. Available gripper model and its dimensions.

reinforced Nylon6 material and pure Nylon6. The production planning was carefully executed with optimal parameters ($A_3B_1C_2$), which was identified as the most favorable in the previous section based on the experimental results, to ensure successful manufacture. Following production, they were subjected to compression testing using a specialized fixture as shown in Fig. S2. Upon examination of the resulting images, brittle fracture was observed in the structures once again.

The loading-displacement graph obtained from the test results is provided in Fig. 20. Here, the condition of 1 mm displacement and 1.2 safety factor with a load of 180 N is indicated. In addition, samples 5 and 7 were removed from the test because products could not be obtained in accordance with the design. As seen in Fig. 20, product number 8 fails to meet the design criteria, while the other products meet them. However, product number 9, with full geometric dimensions, provides a load of 177.50 N for 1 mm displacement, which is at the limit. Upon further examination of the figure, it can be observed that product number 9 has high strength.

Following a thorough force analysis of the products and original item, it is observed that products 1, 3, and 4 are the most appropriate choices in terms of load. A company was tasked with providing cost analyses for 1000 units to pinpoint the most advantageous option. Upon reviewing the results, it has been determined that product number 1 is the most optimal choice, considering production time and weight as illustrated in Table 3. Furthermore, it has been observed that it meets the safety factor of 1.2 for carrying force.

Upon examining the table, it is found that while the production cost of product number 1 is $1.5, the original part costs $5.16, resulting in a difference of $3.66 per unit. When evaluating the results over 1000 units, the total difference amounts to $3660. Considering the 10g material difference between the original part and product number 1, a

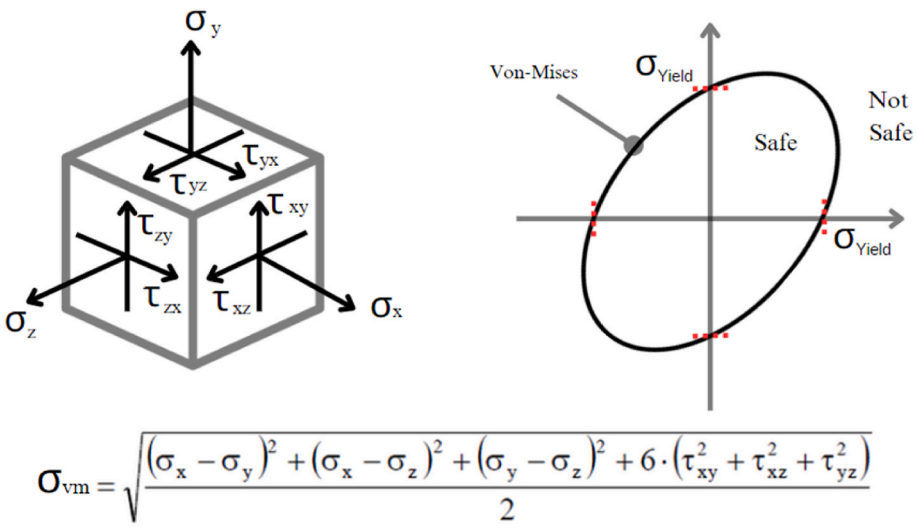

Fig. 18. Von-Mises failure criteria.

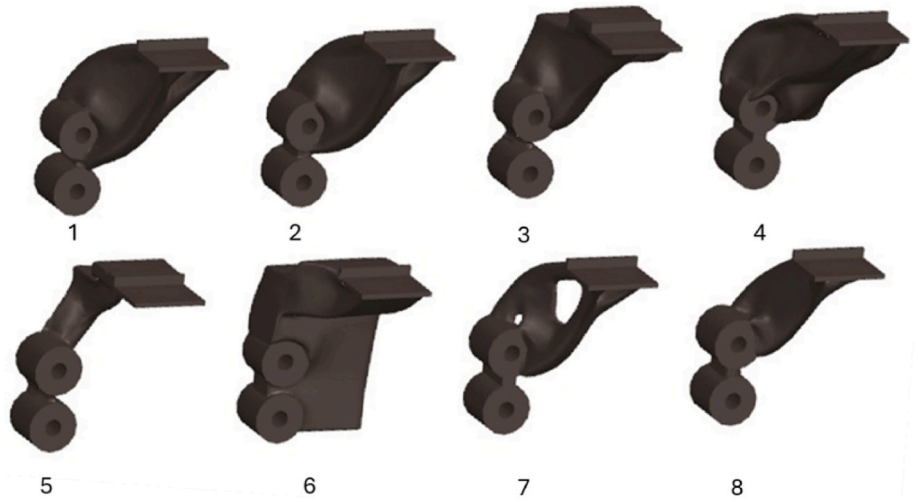

Fig. 19. Redesigned alternative geometries.

material saving of 10,000 g is achieved. This study emphasizes the importance of product development and manufacturing within a scientific framework. It provides an advantage in sustainability due to minimum material waste at the end of this process. This proposed systematic approach will attain significant gains for a sustainable world.

4. Conclusions

This study presents a systematic approach incorporating scientific and practical methodologies for the development of industrial products, supported by a practical case study of gripper design for an industrial robot. At the beginning of the study, it focused on optimizing the production parameters for carbon fiber-reinforced Nylon6, including nozzle temperature, 3D printing speed, and heat treatment time. Key outputs i.e., weight, tensile strength, elongation, elastic modulus, and surface roughness were considered to identify the optimal production levels. The results indicated that the tensile strength increased from 103.2 to 116 MPa which is a notable enhancement of 12.40% attributable to the optimization of production parameters. Similar advancements were observed in other measured properties.

In the second step, this work applied the optimized parameters in an industrial context, utilizing a Generative Design approach to refine the gripper's design. Eight different alternative geometries were generated in addition to the original design, using the mechanical properties derived from the optimized parameters as benchmarks. Then, the geometries were subjected to compression tests, and the observed results were analyzed with a focus on production cost, leading to the selection of the final design. Thanks to optimal design, a significant reduction in material usage, lowering the weight from 14 to 4 g was achieved. In addition, this reduction not only decreased the production cost from $5.16 to $1.50 but also reduced the production time from 58 to 28 min. This means that cost and production time are reduced by approximately 71% and 52%, respectively. Therefore, the result is important in terms of sustainability and cost effectiveness, as well as meeting the requirements for load carrying capacity and production efficiency.

In this investigation, the proposed methodology can be guide in achieving critical advantages for new product developments. On the other hand, further studies focusing on the development of new composite materials with varying compositions and additives are needed to further advance. To characterize new materials, parameters such as layer height and other design and manufacturing factors should be taken into account. Lastly, research on interlayer shear stress is also needed to improve the performance and reliability of additively manufactured components, especially in products subjected to torque and shear forces.

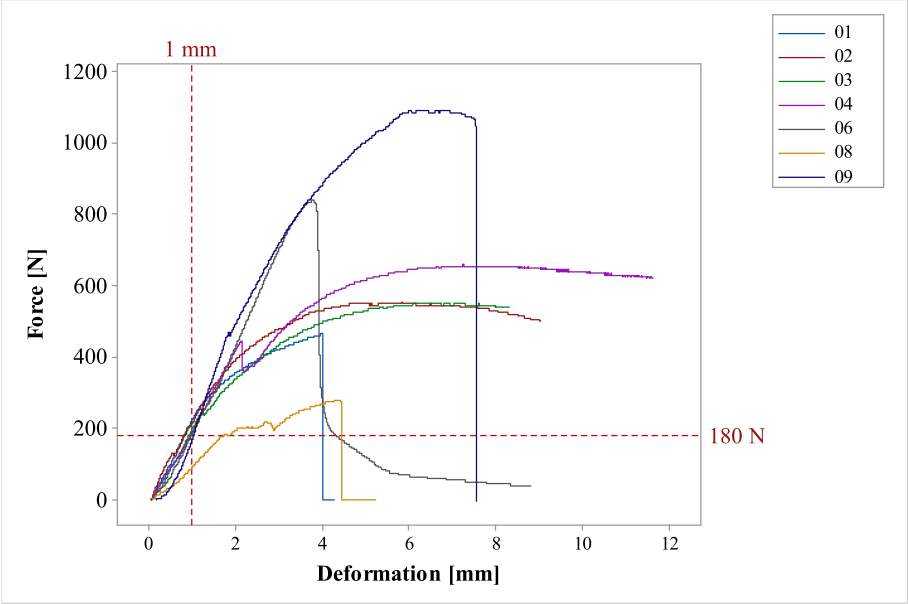

Fig. 20. The loading-displacement graph obtained from the test results.

Declaration of competing interest

The authors declare that they have no known competing financial interests or personal relationships that could have appeared to influence the work reported in this paper.

Acknowledgement

This study has been supported by the Recep Tayyip Erdoğan University Development Foundation (Grant number: 02024009018057)

The authors would like to thank Serkan Uçkan and Barış Bozdemir for enabling the use of the Uçkan Test and Measurement Systems Instron laboratory equipment and facilities.

Murat Sarıkaya acknowledges the Polish National Agency for Academic Exchange (NAWA) under the Ulam Programme (Grant No. BPN/ULM/2023/1/00035).

Appendix A. Supplementary data

Supplementary data to this article can be found online at https://doi.org/10.1016/j.jmrt.2024.10.064.

References

[1] Ngo TD, Kashani A, Imbalzano G, Nguyen KTQ, Hui D. Additive manufacturing (3D printing): a review of materials, methods, applications and challenges. Compos B Eng 2018;143:172–96. https://doi.org/10.1016/j.compositesb.2018.02.012.

[2] Agarwal K, Kuchipudi SK, Girard B, Houser M. Mechanical properties of fiber reinforced polymer composites: a comparative study of conventional and additive manufacturing methods. J Compos Mater 2018;52:3173–81. https://doi.org/10.1177/0021998318762297.

[3] Zhang Z, Yang G, Pan B, Sun M, Zhang G, Chai H, et al. Experimental study and numerical simulation of morphing characteristics of bistable laminates embedded with 3D printed shape memory polymers. Smart Mater Struct 2024;33:055031. https://doi.org/10.1088/1361-665X/ad3d18.

[4] Zhang Z, Xu J, Ma Y, Sun M, Pan B, Chai H, et al. Morphing characteristics and damage analysis of 3D printing variable stiffness bistable laminates based on continuous fiber thermosetting composites. Compos Struct 2023;315:117026. https://doi.org/10.1016/j.compstruct.2023.117026.

[5] Quan Z, Wu A, Keefe M, Qin X, Yu J, Suhr J, et al. Additive manufacturing of multi-directional preforms for composites: opportunities and challenges. Mater Today 2015;18:503–12. https://doi.org/10.1016/j.mattod.2015.05.001.

[6] Zhang Z, Wang S, Ma Y, Pan B, Sun M, Zhang G, et al. Laser-assisted thermoplastic composite automated fiber placement robot for bonding GF/PP unidirectional composites and braided composites. Compos B Eng 2024;287:111798. https://doi.org/10.1016/j.compositesb.2024.111798.

[7] Zhang Z, Xu J, Ma Y, Sun M, Chai H, Wu H, et al. Design and analysis of multistable curvilinear-fiber laminates based on continuous fiber 3D printing of thermosetting resin matrix. Compos Struct 2023;307:116616. https://doi.org/10.1016/j.compstruct.2022.116616.

[8] Asyraf MRM, Ishak MR, Syamsir A, Amir AL, Nurazzi NM, Norrrahim MNF, et al. Filament-wound glass-fibre reinforced polymer composites: potential applications for cross arm structure in transmission towers. Polym Bull 2023;80:1059–84. https://doi.org/10.1007/s00289-022-04114-4.

[9] Uşun A, Gümrük R. The mechanical performance of the 3D printed composites produced with continuous carbon fiber reinforced filaments obtained via melt impregnation. Addit Manuf 2021;46:102112. https://doi.org/10.1016/j.addma.2021.102112.

[10] Cersoli T, Yelamanchi B, MacDonald E, Carrillo JG, Cortes P. 3D printing of a continuous fiber-reinforced composite based on a coaxial Kevlar/PLA filament. Compos Adv Mater 2021;30:26349833211000056. https://doi.org/10.1177/26349833211000058.

[11] Syrlybayev D, Zharylkassyn B, Seisekulova A, Akhmetov M, Perveen A, Talamona D. Optimisation of strength properties of FDM printed parts—a critical review. Polymers 2021;13. https://doi.org/10.3390/polym13101587.

[12] Tran TQ, Ng FL, Kai JTY, Feih S, Nai MLS. Tensile strength enhancement of fused filament fabrication printed parts: a review of process improvement approaches and respective impact. Addit Manuf 2022;54:102724. https://doi.org/10.1016/j.addma.2022.102724.

[13] Lalegani Dezaki M, Mohd Ariffin MKA, Hatami S. An overview of fused deposition modelling (FDM): research, development and process optimisation. Rapid Prototyp J 2021;27:562–82. https://doi.org/10.1108/RPJ-08-2019-0230.

[14] Tutar M. A comparative evaluation of the effects of manufacturing parameters on mechanical properties of additively manufactured PA and CF-reinforced PA materials. Polymers 2023;15. https://doi.org/10.3390/polym15010038.

[15] Condruz M-R, Paraschiv A, Badea T-A, Useriu D, Frigioescu T-F, Badea G, et al. A study on mechanical properties of low-cost thermoplastic-based materials for material extrusion additive manufacturing. Polymers 2023;15. https://doi.org/10.3390/polym15142981.

[16] Távara L, Madrigal C, Aranda MT, Justo J. Anisotropy and ageing effect on the mechanical behaviour of 3D-printed short carbon-fibre composite parts. Compos Struct 2023;321:117196. https://doi.org/10.1016/j.compstruct.2023.117196.

[17] Venkatesh R, Jerold John Britto J, Amudhan K, Anbumalar V, Prabhakaran R, Thiyanesh Sakthi R. Experimental investigation of mechanical properties on CF reinforced PLA, ABS and Nylon composite part. Mater Today Proc 2023;76:647–53. https://doi.org/10.1016/j.matpr.2022.12.091.

[18] Chacón JM, Caminero MA, Núñez PJ, García-Plaza E, García-Moreno I, Reverte JM. Additive manufacturing of continuous fibre reinforced thermoplastic composites using fused deposition modelling: effect of process parameters on mechanical properties. Compos Sci Technol 2019;181:107688. https://doi.org/10.1016/j.compscitech.2019.107688.

[19] Caminero MA, Chacón JM, García-Moreno I, Rodríguez GP. Impact damage resistance of 3D printed continuous fibre reinforced thermoplastic composites using fused deposition modelling. Compos B Eng 2018;148:93–103. https://doi.org/10.1016/j.compositesb.2018.04.054.

[20] Ferreira LM, Aranda MT, Muñoz-Reja M, Coelho CACP, Távara L. Ageing effect on the low-velocity impact response of 3D printed continuous fibre reinforced composites. Compos B Eng 2023;267:111031. https://doi.org/10.1016/j.compositesb.2023.111031.

[21] Ferreira I, Machado M, Alves F, Torres Marques A. A review on fibre reinforced composite printing via FFF. Rapid Prototyp J 2019;25:972–88. https://doi.org/10.1108/RPJ-01-2019-0004.
[22] Prajapati AR, Dave HK, Raval HK. Influence of fiber rings on impact strengthof 3d printed fiber reinforced polymer composite. Manuf Technol 2020;12:157–63.
[23] AlMuhanna M, AlMangour B. Effect of building orientation and fibre type on the mechanical behaviour of additively manufactured ABS matrix composites. Mater Res Innovat 2023;27:482–9. https://doi.org/10.1080/14328917.2023.2196480.
[24] Kabir SMF, Mathur K, Seyam A-FM. Maximizing the performance of 3D printed fiber-reinforced composites. Journal of Composites Science 2021;5. https://doi.org/10.3390/jcs5050136.
[25] Wickramasinghe S, Do T, Tran P. FDM-based 3D printing of polymer and associated composite: a review on mechanical properties, defects and treatments. Polymers 2020;12. https://doi.org/10.3390/polym12071529.
[26] Nagendra J, Prasad MSG. FDM process parameter optimization by Taguchi technique for augmenting the mechanical properties of nylon–aramid composite used as filament material. J Inst Eng: Series C 2020;101:313–22. https://doi.org/10.1007/s40032-019-00538-6.
[27] Junk S, Rothe N. Lightweight design of automotive components using generative design with fiber-reinforced additive manufacturing. Procedia CIRP 2022;109:119–24. https://doi.org/10.1016/j.procir.2022.05.224.
[28] Han L, Du W, Xia Z, Gao B, Yang M. Generative design and integrated 3D printing manufacture of cross joints. Materials 2022;15. https://doi.org/10.3390/ma15144753.
[29] Abbas TF, Ali HB, Mansor KK. Influence of FDM process VARIABLES'ON tensile strength, weight, and actual printing time when using ABS filament. International Journal of Modern Manufacturing Technologies (IJMMT) 2022;14.
[30] Mykhailyshyn R, Duchoň F, Mykhailyshyn M, Majewicz Fey A. Three-dimensional printing of cylindrical nozzle elements of Bernoulli gripping devices for industrial robots. Robotics 2022;11. https://doi.org/10.3390/robotics11060140.
[31] Goh GL, Goh GD, Nguyen VP, Toh W, Lee S, Li X, et al. A 3D printing-enabled artificially innervated smart soft gripper with variable joint stiffness. Adv Mater Technol 2023;8:2301426. https://doi.org/10.1002/admt.202301426.
[32] Xin Y, Zhou X, Bark H, Lee PS. The role of 3D printing technologies in soft grippers. Adv Mater 2024;36:2307963. https://doi.org/10.1002/adma.202307963.